Available online at www.sciencedirect.com

SCIENCE DIRECT®

Earth and Planetary Science Letters 234 (2005) 369–383

EPSL

www.elsevier.com/locate/epsl

Subduction cycling of U, Th, and Pb

Katherine A. Kelley[a,*], Terry Plank[a], Linda Farr[a], John Ludden[b], Hubert Staudigel[c]

[a]*Department of Earth Sciences, Boston University, 685 Commonwealth Ave., Boston, MA 02215, USA*
[b]*CRPG/CNRS Vandoeuvre-lès-Nancy, BP 20, France*
[c]*Institute of Geophysics and Planetary Physics, Scripps Institution of Oceanography, University of California, San Diego, La Jolla, CA 92093-0225, USA*

Received 11 February 2004; received in revised form 29 January 2005; accepted 4 March 2005
Available online 3 May 2005
Editor: K. Farley

Abstract

Many studies argue, based partly on Pb isotopic evidence, that recycled, subducted slabs reside in the mantle source of ocean island basalts (OIB) [1–3] [A.W. Hofmann, W.M. White, Mantle plumes from ancient oceanic crust. Earth Planet. Sci. Lett. 57 (1982) 421–436; B.L. Weaver, The origin of ocean island basalt end-member compositions: trace element and isotopic constraints. Earth Planet. Sci. Lett. 104 (1991) 381–397; J.C. Lassiter, E.H. Hauri, Osmium-isotope variations in Hawaiian lavas: evidence for recycled oceanic lithosphere in the Hawaiian plume, Earth Planet. Sci. Lett. 164 (1998) 483–496]. Such models, however, have remained largely untested against actual subduction zone inputs, due to the scarcity of comprehensive measurements of both radioactive parents (Th and U) and radiogenic daughter (Pb) in altered oceanic crust (AOC). Here, we discuss new, comprehensive measurements of U, Th, and Pb concentrations in the oldest AOC, ODP Site 801, and consider the effect of subducting this crust on the long-term Pb isotope evolution of the mantle. The upper 500 m of AOC at Site 801 shows >4-fold enrichment in U over pristine glass during seafloor alteration, but no net change to Pb or Th. Without subduction zone processing, ancient AOC would evolve to low $^{208}Pb/^{206}Pb$ compositions unobserved in the modern mantle [4] [S.R. Hart, H. Staudigel, Isotopic characterization and identification of recycled components, in: Crust/Mantle Recycling at Convergence Zones, Eds. S.R. Hart, L. Gülen, NATO ASI Series. Series C: Mathematical and Physical Sciences 258, pp. 15–28, D. Reidel Publishing Company, Dordrecht-Boston, 1989]. Subduction, however, drives U–Th–Pb fractionation as AOC dehydrates in the earth's interior. Pacific arcs define mixing trends requiring 8-fold enrichment in Pb over U in AOC-derived fluid. A mass balance across the Mariana subduction zone shows that 44–75% of Pb but <10% of U is lost from AOC to the arc, and a further 10–23% of Pb and 19–40% of U is lost to the back-arc. Pb is lost shallow and U deep from subducted AOC, which may be a consequence of the stability of phases binding these elements during seafloor alteration: U in carbonate and Pb in sulfides. The upper end of these recycling estimates, which reflect maximum arc and back-arc growth rates, remove enough Pb and U from the slab to enable it to evolve rapidly ($\ll 0.5$ Ga) to sources suitable to explain the $^{208}Pb/^{206}Pb$ isotopic array of OIB, although these conditions fail to simultaneously satisfy the $^{207}Pb/^{206}Pb$ system. Lower growth rates would require additional U loss

* Corresponding author. Now at Department of Terrestrial Magnetism, Carnegie Institution of Washington, 5241 Broad Branch Rd., NW, Washington, DC 20015, USA. Tel.: +1 202 478 8475; fax: +1 202 478 8821.
E-mail addresses: kelley@dtm.ciw.edu (K.A. Kelley), tplank@bu.edu (T. Plank), john.ludden@cnrs-dir.fr (J. Ludden), hstaudigel@ucsd.edu (H. Staudigel).

doi:10.1016/j.epsl.2005.03.005

(29%) at depths beyond the zones of arc and back-arc magmagenesis, which would decrease upper mantle κ ($^{232}Th/^{238}U$) over time, consistent with one solution to the "kappa conundrum" [5] [T. Elliott, A. Zindler, B. Bourdon, Exploring the kappa conundrum: the role of recycling in the lead isotope evolution of the mantle. Earth Planet. Sci. Lett. 169 (1999) 129–145]. The net effects of alteration (doubling of μ [$^{238}U/^{204}Pb$]) and subduction (doubling of ω [$^{232}Th/^{204}Pb$]) are sufficient to create the Pb isotopic signatures of oceanic basalts.

Keywords: uranium; thorium; lead; altered oceanic crust; mantle; subduction

1. Introduction

The chemical evolution of the earth's mantle depends on a number of processes, including segregation of the core, extraction of crust, and re-injection of subducted slabs. Of these, the recycling of subducted slabs [1–4] has received much attention towards explaining some unusual geochemical features of ocean island basalts (OIB). At one time, models invoked a sequestered, primordial mantle source for OIB [6,7], but more recent studies (e.g. [8,9]) favor the Hofmann and White [1] model of recycled oceanic crust in the source of hotspot magmas. Altered oceanic crust (AOC) meets many of the source criteria established by OIB geochemistry, particularly U and Re enrichment, which over time could create the radiogenic Pb and Os isotope signatures characteristic of many OIBs [10,11]. Isotopic end-members in OIB suggest links to distinct recycled materials such as pelagic sediment, terrigenous sediment, and AOC [2]. A plethora of geochemical observations (Sr, Nd, Pb, O, H, Os, Hf isotopic compositions and certain trace element ratios) have revealed regional variations in OIB from French Polynesia [12], Hawaii [3,13,14], and Iceland [15] that may relate to distinct portions of recycled subducted crustal packages.

Few of these models, however, have been quantitatively tested against actual crustal inputs to the subduction zone. Moreover, subducted slabs are geochemically processed as they descend through the subduction zone [16–19], which fundamentally modifies the composition of the slab residue that is ultimately transported into the deep earth. The radioactive decay systems of ^{238}U–^{206}Pb, ^{232}Th–^{208}Pb, and ^{235}U–^{207}Pb provide valuable geochemical tools for tracing the evolution of subducting slabs because the three elements appear to partition differently in slab fluids, and the half-lives of the decay systems are large enough to make adequate tracers over the age of the earth. The goal of this work is to develop a quantitative model for Pb isotope evolution in the mantle, incorporating recent measurements of U, Th, and Pb in AOC and arc lavas. Thus far, studies of the U–Th–Pb system have focused on separate phenomena: (1) the Ce/Pb evolution of the earth; (2) high μ ($^{238}U/^{204}Pb$) in OIB; and (3) the upper mantle "kappa ($^{232}Th/^{238}U$) conundrum." We discuss each of these topics below, then consider how to unite them into a single model for the U–Th–Pb system.

Hofmann et al. [20] first demonstrated the high value and relative constancy of Ce/Pb in the oceanic mantle (OIB and mid-ocean ridge basalt [MORB]), in contrast to the distinctly low Ce/Pb values in the continental crust, subduction-related magmas, and the bulk earth. Several studies have since developed quantitative models for the Ce/Pb evolution of the mantle and crust based on mass balance of Ce and Pb across the Aleutian arc [17], experimentally determined partition coefficients for Ce and Pb between high *P–T* aqueous fluids and slab silicates [18], present-day continent and MORB compositions [19], and Pb redistribution in oceanic crust during hydrothermal alteration [21,22]. Together, these studies indicate preferential enrichment of Pb over Ce in arc magmas and the continental crust as a consequence of the hydrothermal mobility of Pb during seafloor alteration and subduction dehydration. These different studies estimate 25–33% loss of the Pb budget in subducting AOC to arc magmas, and ultimately the continental crust, leaving the high Ce/Pb slab residue to mix back into the mantle. The Ce/Pb cycle has thus been quantitatively well described. Similar constraints on the U–Th–Pb cycle would permit forward modeling of Pb isotope evolution in the earth through time, which is the primary goal of this study.

Lead isotopes provide clear evidence that most hotspot magmas do not derive from primordial mantle because they trend to more radiogenic $^{206}Pb/^{204}Pb$ and

$^{207}Pb/^{204}Pb$ compositions than the closed system, meteorite-defined geochron. This observation relates to the classic "Pb paradox," which stems from the observation that both the mantle and continents lie to the right of the geochron [23]. Resolution of the Pb paradox requires a complementary low μ ($^{238}U/^{204}Pb$) reservoir in the Earth (probably the core [24]), but the generation of high μ (HIMU) in the OIB source is a separate problem. The most common explanation for HIMU OIB is subduction recycling of high μ AOC [2,12,25]. While this is a plausible solution that broadly satisfies the two U–Pb isotopic decay systems, it fails to address constraints from the evolution of thorium-derived Pb ($^{208}Pb/^{204}Pb$) and Th/U in the mantle (i.e. the "kappa conundrum").

The discrepancy between the Pb isotopes of MORBs and their present ratio of parent isotopes ($\kappa = {}^{232}Th/^{238}U$) has been dubbed the "kappa conundrum" [5]. Specifically, $^{208}Pb/^{204}Pb$ and $^{206}Pb/^{204}Pb$ in MORB appear to have evolved over time from mantle with higher κ (i.e. κ_{Pb}) than the lavas record today [26,27]. One general solution to the kappa conundrum is to decrease κ in the upper mantle, either through continent extraction [27,28] or uranium addition from subducting slabs [5]. Successful solutions for the kappa conundrum, however, must be consistent with Ce/Pb and Pb isotopic constraints from other earth reservoirs.

Several models independently explain Ce/Pb, HIMU, and kappa, but none yet link all three observations in a single, coherent model for U, Th, and Pb. Resolution of these theories requires constraints on U, Th, and Pb concentrations in subducting AOC, from mid-ocean ridge to the trench and through the subduction zone. Here, we discuss data from a new bulk estimate of AOC and evaluate how compositions of the slab, arc crust, and upper mantle change as subducted crust advances through the earth's interior.

2. Prior work on altered oceanic crust

Our current understanding of the bulk composition of old AOC comes largely from a single location, DSDP Site 417/418, which is the only well-studied, high-recovery (>50%) drill site that penetrates deeply (>500 m) into slow-spreading, 118 Ma Atlantic crust [29]. The Site 417/418 data provide a primary reference for the geochemical effects of long-term seafloor alteration on the composition of oceanic crust [4,29,30]. Another well-studied drill site, DSDP/ODP Hole 504B, situated in young (~7 Ma) Costa Rica Rift crust, is the deepest-penetrating basement hole in the oceans (1.8 km) and provides a reference for young AOC [31,32]. Hole 504B is also the only location where drilling has provided an in situ section through both extrusive pillows and flows and underlying dikes.

Hart and Staudigel [4] used Site 417/418 data to develop a Pb isotope evolution model demonstrating how AOC, subducted continually throughout Earth history, would evolve to the present day. This model consists of multiple, three-stage Pb isotope growth models (modified from the two-stage model of [33]) that initiate the third stage at different times through earth history, illustrating the continuous addition of material of constant composition into a reservoir isolated from the rest of the mantle (Fig. 1). At any time in Earth history, oceanic crust with the Pb isotopic composition of the mantle is enriched in U through seafloor alteration and then is "subducted" into the isolated reservoir. The parent isotopes of U and Th decay to Pb isotopes that reflect both the time of AOC subduction and the starting parent/daughter ratios: μ ($^{238}U/^{204}Pb$), and ω ($^{232}Th/^{204}Pb$). At present, AOC that has been continuously added to this reservoir should fall along an array formed by a line connecting each of these curves at $t=0$ (Fig. 1). Hart and Staudigel [4] used this model with the data from Sites 417/418 to show that AOC will evolve through time to a Pb isotopic composition that does not resemble any oceanic basalt (line A, Fig. 2a,b). This result derives from a large increase in μ with a simultaneous decrease in ω for Site 417/418 AOC. Altered MORB with these parent/daughter characteristics will evolve to very low $^{208}Pb/^{206}Pb$ compared with the modern oceanic mantle.

Bach et al. [32] reached a similar conclusion for the bulk composition of Hole 504B, but also evaluated how this crust must change in order to make a viable precursor to HIMU. They concluded that AOC at Hole 504B must lose 80–90% Pb and 35–40% U in order to create a composition that will develop a HIMU signature in 1–2 Ga. While some losses are expected during subduction-driven dehydration, Bach et al. [32] note a significant discrepancy between their

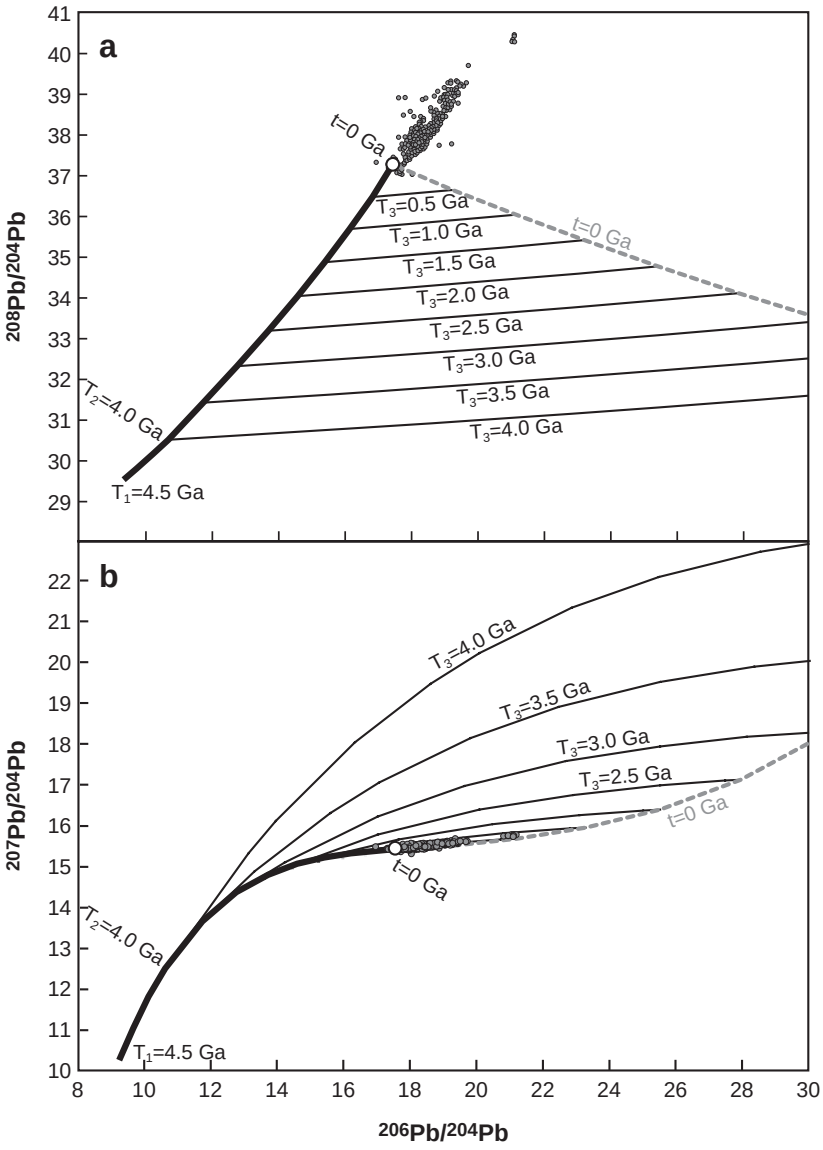

Fig. 1. Growth curves for (a) $^{208}Pb/^{204}Pb$ and (b) $^{207}Pb/^{204}Pb$ vs. $^{206}Pb/^{204}Pb$ used to construct the Pb isotope evolution models [4] in Fig. 2. Thick black line is a simple, two-stage growth curve [33], beginning the first stage at $T_1=4.5$ Ga and the second stage at $T_2=4.0$ Ga. The endpoint at $t=0$ Ga on the two-stage curve represents the model position of the least radiogenic MORB at the present day (DMM). Conditions for stages 1 and 2 are provided in Table 1. Three-stage growth curves are shown as thin black lines, which follow the two-stage curve until initiation of the third stage at T_3 in 0.5 Ga intervals. Each three-stage curve represents the growth curve followed by oceanic crust derived from the MORB mantle at some time in the past (T_3), geochemically modified through alteration and/or subduction, and then sequestered until the present ($t=0$) to allow ingrowth of radiogenic Pb [4]. The dashed line connects the two- and three-stage curves at $t=0$ (present day) to show the trend of the isotopic array of crust of a given composition continually subducted throughout Earth history, as in Fig. 2. All three-stage curves derive from constant μ and ω (from the 417/418 Super composite [4]; Table 1). Gray circles are MORB and OIB [5].

calculated Pb losses from the slab (80–90%) and those determined through other means (i.e. 25–33% from Ce/Pb; see above).

There are, however, two major points to consider before abandoning the subducted slab model for OIB. First, data from Sites 417/418 and 504 may not

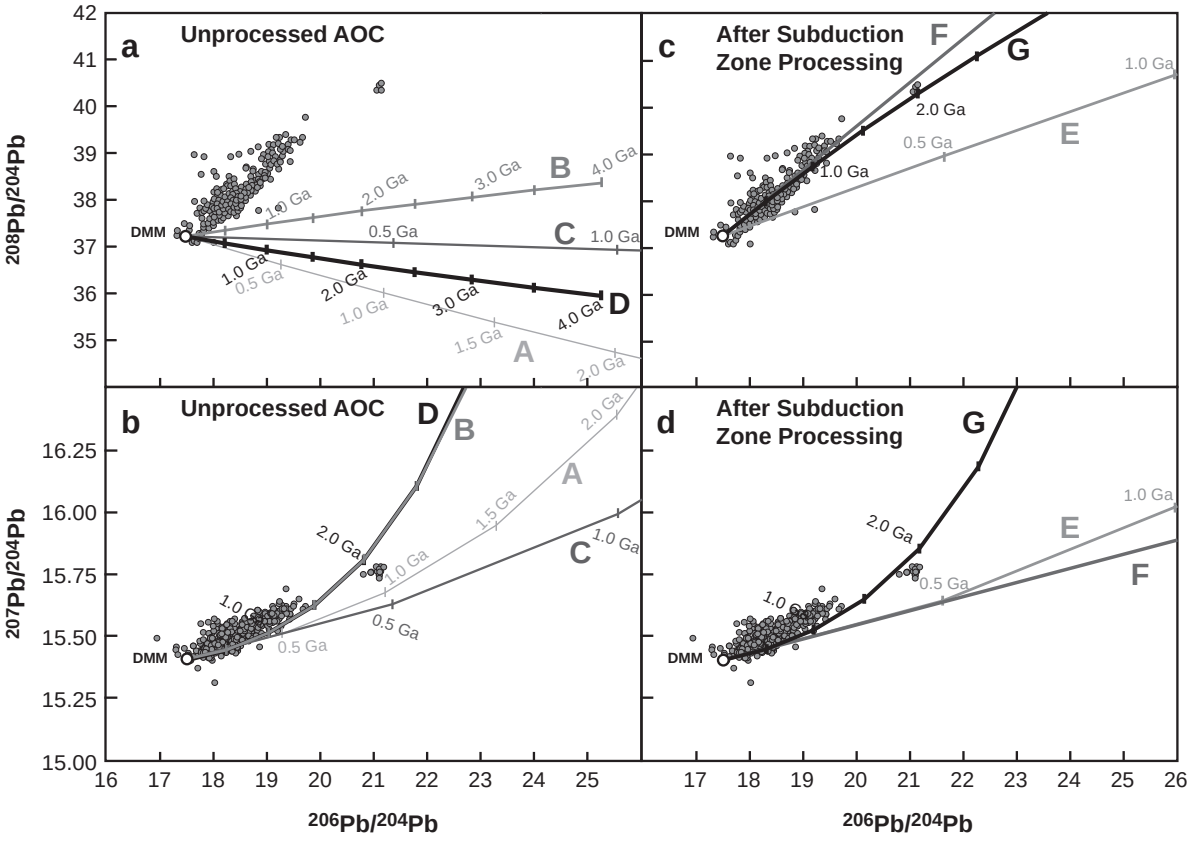

Fig. 2. Pb isotope evolution model [4] (see Fig. 1 for detail). Tick marks indicate the sequestration age of the oceanic crust (T_3). Small gray circles are MORB and OIB [5]. Models of bulk altered oceanic crust in (a) $^{208}Pb/^{204}Pb$ and (b) $^{207}Pb/^{204}Pb$ vs. $^{206}Pb/^{204}Pb$. Line A is as for Fig. 1, for the DSDP Site 417/418 Super composite (500 m) [4], line B is the DSDP/ODP Hole 504B volcanic zone (500 m) [32], line C is the ODP Site 801 Super composite (500 m), line D is ODP Site 801 (6 km; see Table 1). ODP Site 801 AOC (6 km) after subduction zone processing in (c) $^{208}Pb/^{204}Pb$ and (d) $^{207}Pb/^{204}Pb$ vs. $^{206}Pb/^{204}Pb$. Line E is the residual slab after processing through the arc at maximum crustal growth (lost 75% Pb, 10% U), line F is the residual slab after processing through the arc and back-arc at maximum crustal growth (lost 98% Pb, 50% U), line G is from model OIB reservoir parameters [5] (equivalent to slab losses of 58% Pb and 54% U).

accurately reflect the composition of global subducting AOC, and second, the U–Th–Pb systematics in arc magmas independently constrain the further processing of AOC during subduction. We address both issues here.

3. Samples and methods

The young age and poor recovery at Hole 504B and lead contamination suffered by Site 417/418 samples ([4]; see Table 1) raise questions about their suitability for studies of U–Th–Pb cycling. Here, we evaluate new data from ODP Site 801, a recently drilled sequence of fast-spreading, Jurassic MORB (170 Ma [34]) in the western Pacific Ocean. Initiated during ODP Leg 129 [35] and continued during Leg 185 [34], drilling at Site 801 penetrated 470 m into basement, sampling most of the extrusive sequence of crust. Site 801 is not only ideally situated relative to the well-studied Mariana island arc system, but since it is the only deeply drilled site in old, fast-spreading Pacific crust, Site 801 is also an appropriate basement reference site for much of the global subduction flux.

Estimation of the bulk composition of Site 801 comprises inductively coupled plasma mass spectrometry (ICP-MS) analyses of 79 discrete and 10 mixed composite samples. Sample descriptions, sam-

Table 1
Composition of subducting crust and mass balance results

	Pb (ppm)	Th (ppm)	U (ppm)	μ ($^{238}U/^{204}Pb$)	ω ($^{232}Th/^{204}Pb$)	κ ($^{232}Th/^{238}U$)	Pb lost	U lost
Pb isotope model Stage 1 [4,5]				8.2	29.0	3.6		
Pb isotope model Stage 2 [4,5]				8.0	30.8	3.9		
417/418 fresh [4]	0.28	0.063	0.035					
417/418 Super [4][a]	0.69	0.0723	0.321	30	7	0.23		
504B fresh [32][b]	*0.232*	*0.11*	0.016					
504B VZ Super [32]	0.232	0.11	0.055	17	36	2.1		
801 Primitive Glass (42R2-116; [36])	0.284	0.111	0.044					
801 Dikes (28R1-118; [36])	0.380	0.179	0.088					
801 Gabbro[c]	0.213	0.049	0.011					
801 Super [36]	0.437	0.173	0.390	56	25	0.45		
801, 6 km[d]	0.241	0.092	0.062	17	25	1.5		
Mariana Arc (Gug9; [45])	2.03	0.271	0.147					
Mariana Arc Mantle	0.225	0.030	0.016					
Mariana Arc MORB Mantle [51]	0.019	0.004	0.001					
Mariana Trough (T780:1-3; [55])	0.78	0.36	0.14					
Mariana Trough Mantle	0.045	0.021	0.011					
Mariana Trough MORB Mantle [51]	0.032	0.015	0.005					
Required for OIB [5]				18	60	3.3	58%	54%
Slab post-arc (29–50 km^3/Ma/km [52,53])	0.136–0.060 (0.125)	0.092	0.059–0.056 (0.058)	27–59 (29)	44–100 (48)	1.6–1.7 (1.6)	44–75% (48%)	5.5–9.6% (6.1%)
Slab post-back-arc (83–178 km^3/Ma/km [47])	0.110–0.004 (0.099)	0.092	0.047–0.031 (0.047)	27–445 (30)	54–1354 (60)	2.0–3.0 (2.0)	10–23% (10%)	19–40% (19%)
Slab post-deeper losses							4–0% (0%)	30–0% (29%)

Losses reported as % of original 6 km crustal input. Values in parenthesis indicate preferred values for crustal growth rates of 32 and 83 km^3 / Ma/km for the arc and back-arc. Preferred arc growth rate is average of Reymer and Schubert [52] rates, preferred back-arc rate constrained to make $\omega = 60$ in slab residue.

[a] Many of the 417/418 samples suffered Pb contamination, thus Hart and Staudigel [4] used a Pb value (underlined) derived from a subset of samples inferred to have avoided contamination.

[b] U value is from Site 504 "precursor" composition, Th and Pb (italicized) are assumed to be unchanged in bulk upper 500 m during alteration.

[c] Calculated by summing 2 km of 801 dikes and 4 km of gabbro to a Fo_{89} liquid back-calculated from the primitive glass composition (see text).

[d] Sum of 0.5 km of 801 Super, 1.5 km of 801 dikes and 4 km of 801 gabbro (see text).

pling and analytical methods, and major and trace element data for Site 801 are presented in Kelley et al. [36]. Trace elements in five pristine glass samples were also determined by solution and laser ablation ICP-MS [36,37], and these provide a necessary baseline against which to assess the effects of alteration. The composite samples are physical mixtures of discrete sample powders, combined in the relative proportions of their abundance throughout the core, intended to capture bulk characteristics of large portions of AOC. The composites include averages of less altered and highly altered lithologies, averages of specific depth intervals, and a "Super" composite representing the bulk composition of the full 420 m tholeiitic sequence at Site 801. Similar composites were prepared from Site 417/418 samples [29], and

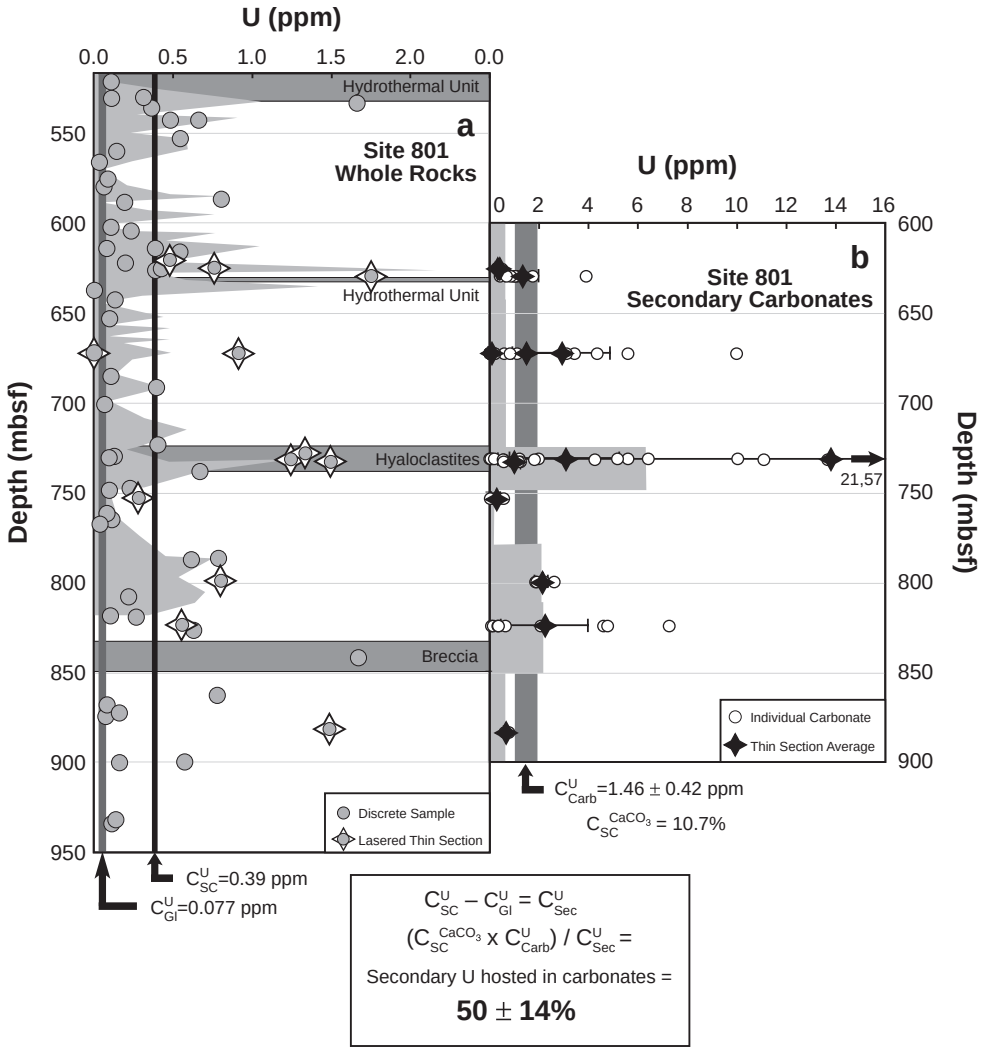

Fig. 3. (a) U concentration vs. depth at Site 801, modified from Kelley et al. [36]. Shaded area traces the general shape of continuous, downhole U concentration recorded by the natural gamma logging tool [34]. Gray circles are discrete, whole-rock samples from the Site 801 core, from Kelley et al. [36]. Samples highlighted with stars are discrete, whole-rock samples from which thin sections were used for laser ablation ICP-MS analyses of alteration phases (see panel b). Zones related to U enrichment (hydrothermal deposits, hyaloclastites, breccia) are highlighted by dark, horizontal bands. Vertical lines indicate bulk U concentrations of average Site 801 glass (0.08 ppm) and the 801 Super composite (0.39 ppm). (b) U concentrations in secondary carbonates vs. depth. Laser-ablation ICP-MS analyses of individual carbonates (open circles), and average carbonates within samples (filled stars), and down-core distribution (guided by logging data; light gray shading). Data, averages, and depth intervals are given in Supplementary Table B. These sample averages are weighted by the length weights given in Supplementary Table B to determine the average for the site (1.46 ppm U on average in carbonates; dark vertical band). Error bars for each sample are 2σ of the mean of the analyses. The uncertainty on the site average was calculated using a Monte Carlo scheme where each sample average was allowed to vary randomly within its 2σ prior to weighting and calculating site average. The uncertainty quoted ($\pm$ 0.42 ppm) represents the full range in 90% of the trials. Box calculation shows how we estimate the proportion of carbonate-bound U that is added by alteration. C^U and C^{CaCO3} are concentrations of U and $CaCO_3$ in different phases, subscript SC is 801 Super composite, Gl is average 801 glass, Carb is average 801 carbonate. Value for $CaCO_3$ in the 801 Super composite from [64].

equivalent weighted averages were calculated for Hole 504B [32], making these three locations directly comparable. We adopt the compositions denoted "Super composite" as representative of the upper 500 m at Sites 417/418 and 801, and "volcanic zone" for the upper 500 m at Site 504.

To determine the mineral hosts of secondary U at Site 801, 12 thin sections were also analyzed by laser ablation ICP-MS at Boston University. Samples are largely from the high-U discrete samples reported in [36], and span most of the 420 m tholeiitic section of the site (Fig. 3a). Uranium and 20 other trace elements were measured by rastering a 50-μm beam across the thin sections. A significant portion of the U is hosted in secondary carbonates, and we report 83 analyses of the major and trace element compositions of ankerite and calcite in Supplementary Tables A and B. Laser ablation ICP-MS detection limits were <1 ppb, and spot-to-spot precision was <4% RSD for U. Time-resolved laser data were reduced using ^{43}Ca as an internal standard, and NIST 612 glass as the external calibration standard. Further details can be found in Supplementary Table B and Farr [38].

4. Results

To illustrate the small-scale geochemical variations at Site 801, as well as the effectiveness of the composites at capturing the characteristics of AOC, we plot Nb, Pb, and U vs. Th for discrete and composite samples (Fig. 4). Both Th and Nb appear immobile and unaffected by alteration (Fig. 4a), illustrated by average NMORB Nb/Th ratios of glass, discrete samples, and composites. The discrete sample data show that alteration redistributes Pb (Fig. 4b), but the average Pb/Th of the composites is within 10% of fresh glass and average NMORB, suggesting Pb is redistributed locally with little to no net change in the top 500 m of AOC. Uranium, however, is clearly enriched in most discrete samples and all of the composites (Fig. 4c). The 801 Super composite indicates a bulk 4.4-fold enrichment of U over pristine glass (0.39 ppm bulk vs. 0.09 ppm average glass) in the upper 500 m of oceanic crust (Fig. 3a) that is consistent with the log-derived bulk U concentration (0.4 ppm [39]). Bulk U enrichment creates high μ (^{238}U/^{204}Pb; μ_{801}=56 (Table 1), μ_{DMM}=8 [4]), but

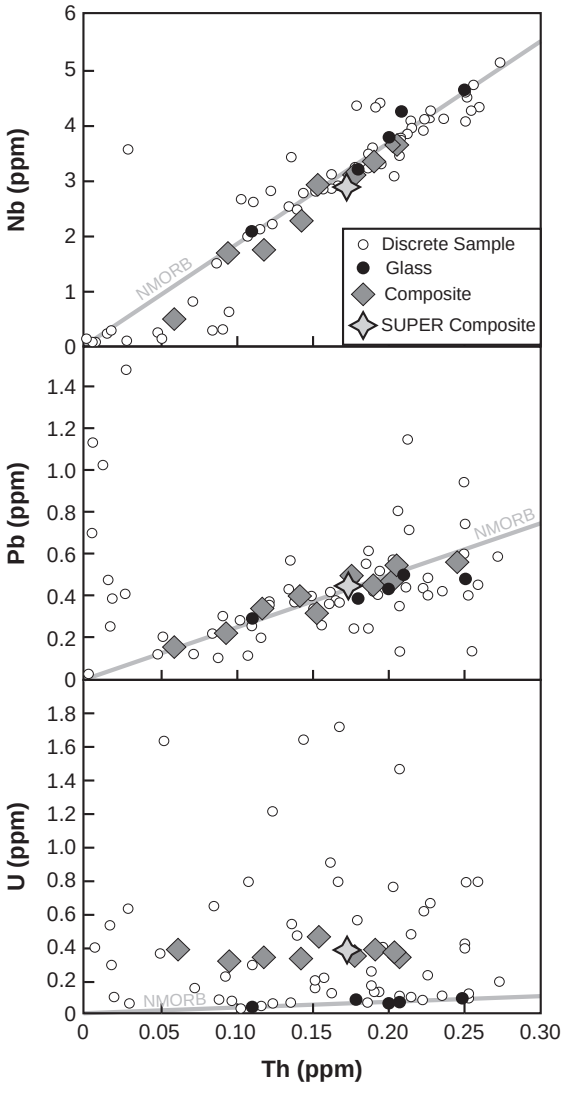

Fig. 4. Nb, Pb, and U vs. Th in ODP Site 801 samples. Data for discrete samples, composites, and glass from Kelley et al. [36]. Gray lines are NMORB ratios from Sun and McDonough [65].

leaves ω (^{232}Th/^{204}Pb) close to a typical mantle value (ω_{801}=25 (Table 1), ω_{DMM}=30 [4]).

The U enrichment at Site 801 is widespread, but does not vary simply as a function of depth or alteration mineralogy. Laser ablation-ICPMS rasters of thin sections show high U concentrations in both secondary carbonates and redox haloes proximal to veins [38], supporting prior work linking U uptake in altered basalt to carbonate (e.g. [29]) and iron oxidation (e.g. [40]). Different generations of carbo-

nate have different U contents, from <0.1 to >50 ppm U (see Supplementary Table B and Fig. 3). The high U carbonates have high Sr and REE patterns similar to seawater, clearly implicating a seawater source of U. The low U carbonates have REE patterns similar to basalt, suggesting they precipitated from fluids that interacted extensively with the host rocks and lost U along the pathway. These different types of carbonates are distributed through the core, presumably as different generations of carbonate precipitated during the 170 Ma history of the site, consistent with cross-cutting relationships [41] and Pb isotope model ages [42]. High-U carbonates predominate in the zone at 725 mbsf, filling primary porosity within hyaloclastites that contain fresh basaltic glass. A significant amount of U is also found in alteration haloes surrounding veins. We find the highest U precipitated well away from the veins, in the boundary between oxidized (celadonite-rich) and reduced (saponite/pyrite-rich) haloes [38]. This distribution suggests processes similar to roll-front deposits, where U (VI) is mobilized from oxidized regions proximal to veins, and precipitated as U (V or IV) oxides when reaching distal reduced portions of the rock. Redox haloes predominate deep in the core (>850 mbsf), creating U-enriched regions in the absence of high U carbonates.

Uranium enrichment of the extrusive basalts at Site 801 (0.39 ppm bulk vs. 0.09 ppm glass; Table 1) is comparable to that estimated at 118 Ma Site 417/418 (0.321 ppm bulk vs. 0.035 ppm fresh [4]; Table 1), but is considerably greater than the enrichment determined at 7 Ma Hole 504B (0.055 ppm bulk vs. 0.016 ppm fresh [32]; Table 1). These observations support the prediction that carbonate precipitation occurs throughout the history of a site [43], and is a major host of secondary U. Thus, unlike other aspects of seafloor alteration (e.g. Rb/Sr and $\delta^{18}O$), which are thought to form within a few Ma after formation of the oceanic crust [43], U enrichment may continually increase with crustal age.

The extrusive sequence of oceanic crust, however, is a thin layer overlying ~6 km of total crust, comprising 2 km of volcanics (0.5 km pillows and flows, 1.5 km dikes) and 4 km of gabbros. While the upper 500 m may be the most intense focus of alteration, by mass it is <1/12 of the total crust. A 6 km sequence of crust should sum to a mantle-derived melt (in equilibrium with Fo_{89}) that has differentiated into gabbros, dikes, and pillows and undergone variable extents of alteration. We estimate the 6 km bulk composition of AOC at Site 801 by first back-calculating the most primitive glass (42R2-116 [37]; Table 1) to a mantle melt by adding equilibrium olivine in 1% increments until Fo_{89} equilibrium is reached (17% total olivine added). This yields a primary bulk composition of the total crust, prior to any alteration. This primary bulk composition may then be segregated into gabbroic and eruptive constituents by assuming the upper 2 km consists of an average glass composition (28R2-118 [37]; Table 1) and the geochemical remainder is distributed over 4 km of gabbro (Table 1). In essence, for a given element, $C^i_B = 0.33(C^i_V) + 0.66(C^i_G)$, where C^i is the concentration of element i, and subscripts B, V, and G refer to bulk (i.e. 42R2-116), volcanic (i.e. 28R2-118), and gabbro, respectively. To determine the bulk composition of 6 km of AOC (Table 1), we recalculate the bulk 6 km using 4 km (66%) of gabbro, 1.5 km (25%) of average glass (28R2-118; equivalent to unaltered dikes), and 0.5 km (8%) of Site 801 Super composite. We assume that Pb and Th are both conserved in the bulk crust during alteration of the dikes and gabbros. Although Pb is clearly redistributed during alteration [21,22], it remains within the crustal package that is consumed at subduction zones. Lead and thorium are therefore roughly equal to their initial concentrations in the bulk crust (Table 1), and enrichment of U in the gabbros and dikes is considered negligible [32,44]. The full 6 km sequence of AOC is, however, enriched in U by a factor of 1.7, which is the result of alteration in the upper 500 m.

5. Discussion

Revisiting the Hart and Staudigel [4] calculation for each of the three AOC estimates, we find that our new AOC composition does not fundamentally change the earlier conclusions. Subducting AOC wholesale into the mantle at various times past still creates negatively sloping (or sub-horizontal) arrays with low $^{208}Pb/^{204}Pb$ relative to $^{206}Pb/^{204}Pb$ (Fig. 2a) quite different from any oceanic basalt. Consideration of a full 6 km sequence of crust does not change this result (Fig. 2a,b, line D). AOC thus must be chemi-

cally processed by subduction, with the net effect of increasing ω in the slab (achieved in practice by mobilizing Pb and U) if it is to contribute significantly to the OIB source.

The net effects of subduction on the U–Th–Pb composition of the slab have never been simple to deduce from the compositions of arc basalts, which are enriched over mid-ocean ridge basalts (MORBs) in each of these elements. All three elements are recycled from the slab to the arc, but of particular importance is the relative fractionation of each from the others. For example, distinctive low Ce/Pb ratios and U-series studies indicating ^{238}U excesses in arc lavas (e.g. [45]) have always pointed to Pb and U mobility in subduction zones, but which is more mobile? Part of the dilemma in interpreting the origins of U, Th, and Pb enrichments in arc lavas arises from mixed contributions of sediment- and AOC-derived components. Using only high-quality ICP-MS data, we find that Pacific arcs define two-component mixing arrays (Fig. 5). These arrays are most likely controlled by mixing of subducted components, shown for example by the Pb isotopic composition of arc basalts [17] and strong global linkages between the Th compositions of incoming sediments at trenches and arc volcanics [46]. One end-member is arc-specific, variably enriched in Th, and probably derived from subducted sediment. The other, presumably AOC-derived, is more uniform, low in Th, high in Pb, and much higher in Pb/U (and thus lower in μ) than AOC itself. Subtracting the contribution from sediment resolves the fractionations of U, Th, and Pb in the AOC-derived fluid that contributes to the arc.

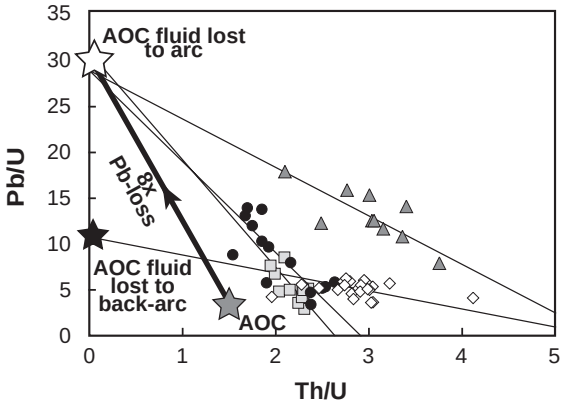

Fig. 5. Pb/U vs. Th/U in arc lavas (all ICP-MS data). Dark gray triangles are Honshu [66], light gray squares are Aleutians [67], black circles are Marianas [45], open diamonds are Mariana back-arc [55]. Thin black lines are RMA linear regressions through data. Thick black line illustrates the difference between bulk AOC and the AOC-derived fluid.

The mixing relationships in Fig. 5 support the idea that a primary source of variability in arc magmas stems from differences in the subducting sediment column at each trench [47], while AOC contributes a more uniform composition. This notion is also consistent with the arc basalt/sediment flux correlation diagrams of Plank and Langmuir [46], where sediment flux controls the trend and AOC flux controls the intercept at zero sediment. For some elements, such as Ba, the intercept (Ba/Na) is highly enriched over MORB, implying significant addition of Ba from the AOC. For others, such as Th, it is not, implying negligible AOC-derived Th (and a dominance due to the sediment Th flux). In the following calculations, we therefore assume that AOC contributes zero Th to the arc, which means our estimates of U and Pb losses are minima and would be greater if Th were mobile. By assuming Th is perfectly immobile, the Pacific arcs in Fig. 5 indicate that Pb is extracted ~8 times more than U from AOC into the AOC-derived fluid (i.e. $[Pb/U_{fluid}]/[Pb/U_{AOC}] = 30/4 = 7.7$). Preferential Pb loss from AOC will increase both μ and ω in the slab residue, which moves compositions in the right direction towards creating the OIB source (Fig. 2b).

We determine actual slab losses through mass balance at the Mariana trench, where inputs and outputs are well-constrained [36,45,48]. Input fluxes to the Mariana trench are calculated by multiplying oceanic crustal thickness (6 km) by density (2.8 g/cm^3 for volcanics, 3.0 g/cm^3 for gabbro) [49], convergence rate (5.475 cm/yr [50]), and concentration of U, Th, and Pb (Table 1), yielding fluxes of 243 g/yr/m arc length Pb, 91 g/yr/m arc length Th, and 54 g/yr/m arc length U. Output fluxes at the Mariana volcanic arc are determined by starting with a Mariana lava with the greatest AOC component and least sediment component (sample Gug9 [45]; Table 1), then converting it to a primary mantle melt by adding 35% olivine (to equilibrium with Fo_{89}; see above) and then calculating from it a mantle source composition by assuming batch melting and $F = 15\%$ (based on Na_2O; Table 1). This arc mantle composition reflects a mixture of three components: MORB-like mantle,

sediment, and AOC-derived fluid. We remove U, Th, and Pb contributions from the sediment to the arc mantle by first subtracting appropriate, depleted MORB mantle Pb, Th, and U concentrations (Table 1; [51]) from the arc mantle concentrations, then assuming all Th in excess of the MORB mantle is sediment-derived (i.e. $C_S^{Th}=C_{AM}^{Th}-C_{MM}^{Th}$, where C^{Th} is the concentration of Th, and subscripts S, AM, and MM refer to sediment component, arc mantle, and MORB mantle, respectively). We then choose Mariana sediment component characteristics consistent with sediment Th/U from [45] and Fig. 5 (Th/U=2.8 and Pb/U=1.1), and use C_S^{Th} to determine C_S^{Pb} and C_S^{U}. These sediment contributions are then subtracted from the sediment+fluid concentrations remaining after the initial subtraction of the MORB mantle, leaving the concentrations of U and Pb contributed to the arc mantle by the AOC-derived fluid. To convert these equivalent mantle concentrations into arc output fluxes, we divide the fluid concentrations by F (15%) and multiply by arc crustal growth rates [52,53] (Table 1), which are the largest source of error and are currently not known within a factor of 2. These calculations indicate that the altered oceanic crust contributes 106–183 g/yr/m arc length Pb and 3.0–5.1 g/yr/m arc length U to the Mariana arc crust. Dividing these output fluxes by the AOC input flux yields the total recycling efficiency: 44–75% of Pb and 6–10% of U lost from AOC to the Mariana arc (Fig. 2b).

Arcs, however, are not the only locations of mass transfer from the slab to the surface. Fore-arc serpentinite mud volcanoes and the back-arc lavas in the Mariana Trough also include chemical components derived from the slab. Transfer of U, Th, or Pb from the slab to the fore-arc is negligible, since these elements are not enriched in fore-arc serpentinites [54]. We calculate the AOC flux to the back-arc in the same way as the arc (see above), using a back-arc lava with characteristics closest to AOC-derived fluid (Sample T780:1-3 [55]; Fig. 5), adding back 10% equilibrium olivine, and assuming F=10% (Table 1) and a MORB mantle composition appropriate for the back-arc (Table 1; [51]). We subtract sediment contributions in the same way (using Th/U=5 and Pb/U=0.9 from Fig. 5), and with appropriate back-arc spreading rates [47] (Table 1), estimate AOC-derived output fluxes for U and Pb at the Mariana Trough. We calculate a smaller loss of Pb (10–23%) and a greater loss of U (19–40%) at the back-arc relative to the arc. Fig. 5 illustrates two main observations quantified by these calculations, one of preferential loss of Pb over U during subduction (54–98% Pb loss vs. 25–50% U loss from AOC), and the other of an inferred depth dependence to Pb and U loss (Pb is mostly lost shallow to the arc, and U is mostly lost deeper to the back-arc).

Our estimate of Pb loss from subducted AOC (54–98%) is greater than prior estimates (29–33% [17–19,21,22]). This is partly because our estimates include both the arc and back-arc contributions; if we compare only the Pb losses to the arc (44–75%), then our results are somewhat closer to the prior range. Indeed, one might argue that back-arc spreading centers are rare and, while relevant to the mass balance in the Marianas, might not be pertinent to a global calculation. On the other hand, back-arc magmas bring material to the surface that is lost from the slab and could otherwise remain in the upper mantle, and should perhaps be considered in models for the evolution of the deeper mantle and residual slab. Using our full estimates for Pb loss from AOC (54–98%), and assuming all of this Pb remains sequestered from the upper mantle, the Ce/Pb evolution of the mantle from 4.5 Ga would proceed too quickly beyond the observed modern MORB Ce/Pb of 25 to values between 50 and 197 at the present day [19]. This discrepancy suggests that (1) lower crustal growth rates are more consistent with constraints from Ce/Pb and (2) some Pb lost from the slab, particularly beneath the back-arc region, could become re-incorporated into the upper mantle. If we consider only Pb losses to the arc (44–75%), the mantle Ce/Pb would proceed to lower values (38–96), though still too high for modern MORB. We note, however, that the Ce/Pb evolution curves for Pb recycling at lower arc growth rates (29–36 km^3/My/km arc length [52]; 44–54% Pb loss) intersect the modern Ce/Pb value of 25 at 1.5–2.0 Ga before the present. If modern-analog subduction processes that efficiently remove Pb relative to Ce from subducted crust initiated at a later stage in earth history (e.g. 3.0–2.5 Ga, instead of 4.5 Ga), then high recycling rates for Pb are fully consistent with mantle Ce/Pb evolution. The effect of higher Pb loss on mantle Ce/Pb could, alternatively, be balanced by low Ce/Pb

sediment that often accompanies AOC into the mantle, although we do not quantitatively address the consequences of sediment addition to the isotopic balance in this model.

Our estimates of the Pb and U losses from AOC to the arc and back-arc not only quantify the sense of Pb–U fractionation in the subduction zone, but also allow predictions of the long-term effects of this process on mantle Pb isotopes. Preferential loss of Pb to the arc relative to U and Th moves the residual slab in the right direction towards creating the OIB array, but losses to the arc alone are insufficient to create a composition that will develop HIMU Pb isotope ratios (line E in Fig. 2c,d). Only by selecting extreme, high-end Pb and U losses to both the arc and back-arc (i.e. 98% Pb and 50% U; which correspond to maximum crustal growth rates) will the slab become a viable precursor for HIMU. These maximum growth rates may successfully transform subducted AOC into a reservoir that will evolve very rapidly ($\ll 0.5$ Ga) to the $^{208}Pb/^{206}Pb$ composition of HIMU OIB (line F in Fig. 2c), but obtaining this result by selecting the maximum end of our estimates is not entirely satisfying and is ultimately inconsistent with Ce/Pb (see above) and the $^{207}Pb/^{206}Pb$ system (line F in Fig. 2d; $^{207}Pb/^{204}Pb$ too low for oceanic basalts). We have also not yet addressed the kappa conundrum and, as suggested by Elliott et al. [5], these two issues may be linked. By choosing more conservative estimates of arc and back-arc crustal growth rates (e.g. Table 1), and allowing further losses of U from the slab to the convecting upper mantle, subduction may simultaneously create HIMU and resolve the kappa conundrum (i.e. supply U to the upper mantle, decreasing Th/U over time).

Fig. 6 and Table 1 illustrate this preferred model, which begins with an estimate of losses to the arc (48% Pb and 6% U) that correspond to an average of the lower crustal growth rates of [52] (i.e. 32 km^3/Ma/km arc length; Table 1). We then constrain Pb loss to the back-arc to lie within the range of Pb losses permitted by back-arc spreading rates while satisfying constraints on ω ($^{232}Th/^{204}Pb$) in OIB ($\omega_{OIB}=60$ [5]; Table 1), leading to 10% further Pb loss to the back-arc (58% total; Table 1). Back-arc U losses then derive from this same spreading rate, leading to 19% loss of U to the back-arc (25% total; Table 1). The additional deep U loss (29%) is constrained by the difference

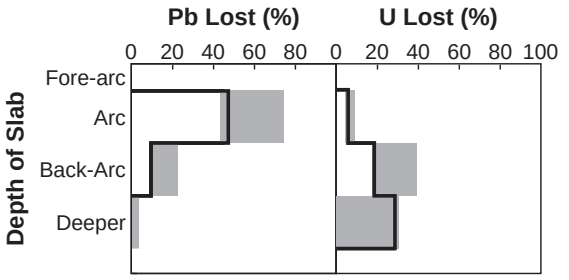

Fig. 6. Slab losses of Pb and U vs. depth in the subduction zone. Gray boxes indicate the full range of possible losses permitted by crustal growth rates. Heavy black line traces slab losses at preferred growth rates (Table 1).

between κ in the starting 6 km AOC and κ in OIB (Table 1; [5]) (i.e. $[1-(\kappa_{AOC}/\kappa_{OIB})]-25\%$). These conditions ultimately satisfy the Pb isotopic constraints on HIMU for all three decay systems (line G, Fig. 2c,d), as well as our mass balance across the Mariana arc. Such deep U release from subducted slabs is also of the right magnitude to solve the kappa conundrum. Assuming 37,000 km of global arc length, our flux calculations indicate that post-arc U loss from AOC supplies a global mass flux of 1×10^9 g/yr of U to the upper mantle, which is the minimum flux required to balance the decrease in upper mantle kappa (from 4.0 to 2.6) over 1.8 Ga [5]. The Nb/U ratio has also steadily decreased in the depleted mantle since ~2.0 Ga, coincident with kappa [56], which further supports the notion that subduction creates a net flux of U into the upper mantle.

High total U losses (54%) contradict current experimental and field constraints on amphibolite/fluid and eclogite/fluid element partitioning [57–60] that suggest Pb is ~10–60 times more mobile than U during slab dehydration. The range of partitioning data is, however, comparable to the relative partitioning indicated by our sub-arc fluid composition, which shows Pb is removed 8× more than U from AOC. These independent experimental and field constrains may therefore be most reflective of shallow, sub-arc processes, and less applicable to deeper slab processing.

Another result of our model calculations is that Pb and U appear to be lost from the slab at different depths (Fig. 6). As the slab descends through the subduction zone, Pb is primarily lost beneath the arc whereas U loss increases with depth. The greatest U loss from the slab, in fact, could take place in the

upper mantle, beyond arc and back-arc magma sources, where no direct magmatic expression exists at the surface. Aside from satisfying the μ and κ constraints, physical evidence from samples of altered oceanic crust also points to the likelihood of deeper U loss. The laser ablation ICP-MS data from alteration phases at Site 801 show that ~50% of the excess U is bound in secondary calcite (Fig. 3; Supplementary Table B). Because 30% of the U in AOC is secondary, then ~15% of the total U in the 6 km bulk AOC is carbonate-hosted. Calcite stability within the subduction zone may exercise a dominant control over U-losses from the slab, whereas sulfide stability may control Pb loss [22]. Carbonates can remain stable deep into the mantle ($\geq$300–400 km depth [61–63]), providing a mechanism to delay U release from the slab. Indeed, the proportion of calcite-bound U at Site 801 (15%) is similar to the deep U loss predicted (29%; Fig. 6). Thus, while originally proposed on the grounds of the kappa conundrum, the deep release of U and the relative partitioning of U, Th, and Pb may be predictable consequences of the different phases that fix and transport these elements in the downgoing plate.

6. Conclusions

The composition of altered oceanic crust, if subducted as-is into the deeper earth, would evolve to Pb isotopic compositions never observed in the modern mantle. This arises because seafloor alteration greatly increases U/Pb (μ) but leaves Th/Pb (ω) essentially unchanged, which greatly perturbs the $^{208}Pb/^{206}Pb$ system. Instead, the chemical fractionations that occur in subduction zones further modify the composition of the slab. The full U–Th–Pb cycle involves a factor of 4.4 increase in U over Pb during seafloor alteration of the upper 500 m of oceanic crust (a factor of 1.7 increase in the full 6 km), an 8-fold loss of Pb over U to the arc, but roughly equal (~55%) overall losses of U and Pb, with no net change to Th, through the subduction process. Seafloor alteration thus doubles μ in 6 km of AOC, whereas subduction doubles ω, generating a composition that can create the Pb isotope signature of OIBs. This work also provides quantitative input for U, Th, and Pb fluxes that may be used in forward models of subduction as a driver of coupled mantle and continent evolution.

The different mineral hosts of U and Pb, and their relative stabilities along the *P–T* path of the slab, cause each element to show a different depth-loss distribution through the subduction zone. Fig. 6 illustrates that there is no single "slab component," and that each element may be used to trace a different aspect of the subduction path. Deep losses of U past the arc and back-arc magmagenesis zones not only provide a solution to the "kappa conundrum," but also may be a natural consequence of the subduction of calcite-bearing altered oceanic crust.

Acknowledgements

Thanks to R. Stern and J. Pearce for sharing their Mariana Trough data, and T. Elliott and S. Goldstein for thoughtful and thorough reviews. We also thank G. Abers, R. Murray, and E. Baxter for constructive comments on this manuscript and the shipboard crew and science party on ODP Leg 185 who made this work possible. This study was supported by a JOI/USSSP grant and an NSF graduate research fellowship.

Appendix A. Supplementary data

Supplementary data associated with this article can be found, in the online version, at doi:10.1016/j.epsl.2005.03.005.

References

[1] A.W. Hofmann, W.M. White, Mantle plumes from ancient oceanic crust, Earth Planet. Sci. Lett. 57 (1982) 421–436.
[2] B.L. Weaver, The origin of ocean island basalt end-member compositions: trace element and isotopic constraints, Earth Planet. Sci. Lett. 104 (1991) 381–397.
[3] J.C. Lassiter, E.H. Hauri, Osmium-isotope variations in Hawaiian lavas: evidence for recycled oceanic lithosphere in the Hawaiian plume, Earth Planet. Sci. Lett. 164 (1998) 483–496.
[4] S.R. Hart, H. Staudigel, Isotopic characterization and identification of recycled components, in: S.R. Hart, L. Gülen (Eds.), Crust/Mantle Recycling at Convergence Zones, NATO ASI Series. Series C, Mathematical and Physical Sciences, vol. 258, D. Reidel Publishing Company, Dordrecht, 1989, pp. 15–28.

[5] T. Elliott, A. Zindler, B. Bourdon, Exploring the kappa conundrum: the role of recycling in the lead isotope evolution of the mantle, Earth Planet. Sci. Lett. 169 (1999) 129–145.
[6] J.-G. Schilling, Iceland mantle plume: geochemical study of the Reykjanes Ridge, Nature 242 (1973) 565–571.
[7] G.J. Wasserburg, D.J. DePaolo, Models of Earth structure inferred from neodymium and strontium isotopic abundances, Proc. Natl. Acad. Sci. U. S. A. 76 (1979) 3594–3598.
[8] A. Stracke, M. Bizimis, V.J.M. Salters, Recycling oceanic crust: quantitative constraints, Geochem. Geophys. Geosyst. 4 (2003).
[9] J.M. Eiler, K.A. Farley, J.W. Valley, A.W. Hofmann, E.M. Stolper, Oxygen isotope constraints on the sources of Hawaiian volcanism, Earth Planet. Sci. Lett. 144 (1996) 453–468.
[10] A. Zindler, S.R. Hart, Chemical geodynamics, Annu. Rev. Earth Planet. Sci. 14 (1986) 493–571.
[11] E.H. Hauri, S.R. Hart, Re–Os isotope systematics of HIMU and EMII oceanic island basalts from the south Pacific Ocean, Earth Planet. Sci. Lett. 114 (1993) 353–371.
[12] C. Chauvel, A.W. Hofmann, P. Vidal, HIMU-EM: the French–Polynesian connection, Earth Planet. Sci. Lett. 110 (1992) 99–119.
[13] J. Blichert-Toft, F.A. Frey, F. Albarède, Hf isotope evidence for pelagic sediments in the source of Hawaiian basalts, Science 285 (1999) 879–882.
[14] A.V. Sobolev, A.W. Hofmann, I.K. Nikogosian, Recycled oceanic crust observed in 'ghost plagioclase' within the source of Mauna Loa lavas, Nature 404 (2000) 986–990.
[15] C. Chauvel, C. Hémond, Melting of a complete section of recycled oceanic crust: trace element and Pb isotopic evidence from Iceland, Geochem. Geophys. Geosyst. 1 (2000).
[16] B.R. Doe, R.E. Zartman, Plumbotectonics, the Phanerozoi, in: H.L. Barnes (Ed.), Geochemistry of Hydrothermal Ore Deposits, Wiley Interscience Publication, New York, 1979, pp. 22–70.
[17] D.M. Miller, S.L. Goldstein, C.H. Langmuir, Cerium/lead and lead isotope ratios in arc magmas and the enrichment of lead in the continents, Nature 368 (1994) 514–519.
[18] J.M. Brenan, H.F. Shaw, F.J. Ryerson, Experimental evidence for the origin of lead enrichment in convergent-margin magmas, Nature 378 (1995) 54–56.
[19] C. Chauvel, S.L. Goldstein, A.W. Hofmann, Hydration and dehydration of oceanic crust controls Pb evolution in the mantle, Chem. Geol. 126 (1995) 65–75.
[20] A.W. Hofmann, K.P. Jochum, M. Seufert, W.M. White, Nb and Pb in oceanic basalts: new constraints on mantle evolution, Earth Planet. Sci. Lett. 79 (1986) 33–45.
[21] B. Peucker-Ehrenbrink, A.W. Hofmann, S.R. Hart, Hydrothermal lead transfer from mantle to continental crust: the role of metalliferous sediments, Earth Planet. Sci. Lett. 125 (1994) 129–142.
[22] R. Mühe, B. Peucker-Ehrenbrink, C.W. Devey, D. Garbe-Schönberg, On the redistribution of Pb in the oceanic crust during hydrothermal alteration, Chem. Geol. 137 (1997) 67–77.
[23] C.J. Allègre, Behavior of U–Th–Pb systems in the upper mantle and a model of the latter's evolution during geologic time, Earth Planet. Sci. Lett. 5 (1969) 261–269.
[24] S.J.G. Galer, S.L. Goldstein, Influence of accretion on lead in the Earth, in: S.R. Hart, A. Basu (Eds.), Reading the Isotopic Code, Geophysical Monograph, vol. 95, American Geophysical Union, Washington, DC, 1996, pp. 75–98.
[25] A.W. Hofmann, Mantle geochemistry: the message from oceanic volcanism, Nature 385 (1997) 219–229.
[26] M. Tatsumoto, R.J. Knight, Isotopic composition of lead in volcanic rocks from central Honshu—with regard to basalt genesis, Geochem. J. 3 (1969) 53–86.
[27] S.J.G. Galer, R.K. O'Nions, Residence time of thorium, uranium and lead in the mantle with implications for mantle convection, Nature 316 (1985) 778–782.
[28] C.J. Allègre, B. Dupré, E. Lewin, Thorium/uranium ratio of the earth, Chem. Geol. 56 (1986) 219–227.
[29] H. Staudigel, T. Plank, B. White, H.-U. Schminke, Geochemical fluxes during seafloor alteration of the basaltic upper oceanic crust: DSDP Sites 417 and 418, Subduction: Top to Bottom Geophysical Monograph, vol. 96, American Geophysical Union, Washington, DC, 1996, pp. 19–38.
[30] H. Staudigel, G.R. Davies, S.R. Hart, K.M. Marchant, B.M. Smith, Large scale isotopic Sr, Nd and O isotopic anatomy of altered oceanic crust: DSDP/ODP sites 417/418, Earth Planet. Sci. Lett. 130 (1995) 169–185.
[31] J.C. Alt, C. Laverne, D.A. Vanko, P. Tartarotti, D. Teagle, A.H.W. Bach, E. Zuegler, J. Erzinger, J. Honnorez, P. Pezard, A.K. Becker, M.H. Salisbury, R.H. Wilkens, Hydrothermal alteration of a section of upper oceanic crust in the eastern equatorial Pacific: a synthesis of results from Site 504 (DSDP Legs 69, 70, and 83, and ODP Legs 111, 137, 140, and 148), in: J.C. Alt, H. Kinoshita, L.B. Stokking, P.J. Michael (Eds.), Proceedings of the Ocean Drilling Program, Scientific Results, vol. 148, 1996, pp. 417–434.
[32] W. Bach, B. Peucker-Ehrenbrink, S.R. Hart, J.S. Blusztajn, Geochemistry of hydrothermally altered oceanic crust: DSDP/ODP Hole 504B—implications for seawater–crust exchange budgets and Sr- and Pb-isotopic evolution of the mantle, Geochem. Geophys. Geosyst. 4 (2003), doi:10.1029/2002GC000419.
[33] J.S. Stacey, J.D. Kramers, Approximation of terrestrial lead isotope evolution by a two-stage model, Earth Planet. Sci. Lett. 26 (1975) 207–221.
[34] T. Plank, J.N. Ludden, C. Escutia, L.J. Abrams, J.C. Alt, R.N. Armstrong, S.R. Barr, A. Bartolini, G. Cairns, M. Fisk, G. Guèrin, S.A. Haveman, T. Hirono, J. Honnoréz, K.A. Kelley, R.L. Larson, F.M. Lozar, R.W. Murray, T.K. Pletsch, R.A. Pockalny, O. Rouxel, A. Schmidt, D.C. Smith, A.J. Spivack, H. Staudigel, M.B. Steiner, R.B. Valentine, Proceedings of the Ocean Drilling Program, Initial Reports, vol. 185, Ocean Drilling Program, College Station, TX, 2000.
[35] Y.P. Lancelot, R.L. Larson, Proceedings of the Ocean Drilling Program, Initial Reports, vol. 129, Ocean Drilling Program, College Station, TX, 1990.
[36] K.A. Kelley, T. Plank, J.N. Ludden, H. Staudigel, Composition of altered oceanic crust at ODP Sites 801 and 1149, Geochem. Geophys. Geosyst. 4 (2003), doi:10.1029/2002GC000435.
[37] M. Fisk, K.A. Kelley, Probing the Pacific's oldest MORB glass: mantle chemistry and melting conditions during the

birth of the Pacific Plate, Earth Planet. Sci. Lett. 202 (2002) 741–752.
[38] L. Farr, The Mineral Hosts of Uranium and the Processes Controlling its Distribution in the Altered Oceanic Crust, Master of Arts, Boston University, 2002.
[39] S. Révillon, S.R. Barr, T.S. Brewer, P.K. Harvey, J. Tarney, An alternative approach using integrated gamma-ray and geochemical data to estimate the inputs to subduction zones from ODP Leg 185, Site 801, Geochem. Geophys. Geosyst. 3 (2002).
[40] W. Bach, J.C. Alt, Y. Niu, S.E. Humphris, J. Erzinger, H.J.B. Dick, The geochemical consequences of late-stage low-grade alteration of lower ocean crust at the SW Indian Ridge: results from ODP Hole 735B (Leg 176), Geochim. Cosmochim. Acta 65 (2001) 3267–3287.
[41] J.C. Alt, D. Teagle, Hydrothermal alteration of upper oceanic crust formed at a fast-spreading ridge: mineral, chemical, and isotopic evidence from ODP Site 801, Chem. Geol. 201 (2003) 191–211.
[42] F. Hauff, K. Hoernle, A. Schmidt, Sr–Nd–Pb composition of Mesozoic Pacific oceanic crust (Site 1149 and 801, ODP Leg 185): implications for alteration of ocean crust and the input into the Izu–Bonin–Mariana subduction system, Geochem. Geophys. Geosyst. 4 (2003), doi:10.1029/2002GC000421.
[43] J.C. Alt, J. Honnorez, C. Laverne, R. Emmermann, Hydrothermal alteration of a 1 km section through the upper oceanic crust, Deep Sea Drilling.25 Project Hole 504B: mineralogy, chemistry, and evolution of seawater–basalt interactions, J. Geophys. Res. 91 (1986) 10309–10355.
[44] S.R. Hart, J. Blusztajn, H.J.B. Dick, P.S. Meyer, K. Muehlenbachs, The fingerprint of seawater circulation in a 500-meter section of ocean crust gabbros, Geochim. Cosmochim. Acta 63 (1999) 4059–4080.
[45] T. Elliott, T. Plank, A. Zindler, W.M. White, B. Bourdon, Element transport from slab to volcanic front at the Mariana arc, J. Geophys. Res. 102 (1997) 14991–15019.
[46] T. Plank, C.H. Langmuir, Tracing trace elements from sediment to volcanic output at subduction zones, Nature 362 (1993) 739–742.
[47] T. Plank, C.H. Langmuir, The chemical composition of subducting sediment and its consequences for the crust and mantle, Chem. Geol. 145 (1998) 325–394.
[48] R.F. Gribble, R.J. Stern, S.H. Bloomer, D. Stuben, T. O'Hearn, S. Newman, MORB mantle and subduction components interact to generate basalts in the southern Mariana Trough back-arc basin, Geochim. Cosmochim. Acta 60 (1996) 2153–2166.
[49] N.I. Christensen, J.D. Smewing, Geology and seismic structure of the northern section of the Oman Ophiolite, J. Geophys. Res. 86 (1981) 2545–2555.
[50] T. Kato, Y. Kotake, S. Nakao, J. Beavan, K. Hirahara, M. Okada, M. Hoshiba, O. Kamigaichi, R.B. Feir, P.H. Park, M.D. Gerasimenko, M. Kasahara, Initial results from WING, the continuous GPS network in the western Pacific area, Geophys. Res. Lett. 25 (1998) 369–372.
[51] Y. Niu, R. Batiza, Trace element evidence from seamounts for recycled oceanic crust in the Eastern Pacific mantle, Earth Planet. Sci. Lett. 148 (1997) 471–483.
[52] A. Reymer, G. Schubert, Phanerozoic addition rates to the continental crust and crustal growth, Tectonics 3 (1984) 63–77.
[53] C. Dimalanta, New rates of western Pacific island arc magmatism from seismic and gravity data, Earth Planet. Sci. Lett. 202 (2002) 105–115.
[54] I.P. Savov, J.G. Ryan, M. D'Antonio, K. Kelly, P. Mattie, Geochemistry of serpentinized peridotites from the Mariana Forearc Conical Seamount, ODP Leg 125: implications for the elemental recycling at subduction zones, Geochem. Geophys. Geosyst. 6 (4) (2005), doi:10.1029/2004GC000777.
[55] J.A. Pearce, R.J. Stern, S.H. Bloomer, P. Fryer, Geochemical mapping of the Mariana arc-basin system: implications for the nature and distribution of subduction components, Geochem. Geophys. Geosyst. (in press).
[56] K.D. Collerson, B.S. Kamber, Evolution of the continents and the atmosphere inferred from Th–U–Nb systematics of the depleted mantle, Science 283 (1999) 1519–1522.
[57] J.M. Brenan, H.F. Shaw, F.J. Ryerson, D.L. Phinney, Mineral-aqueous fluid partitioning of trace elements at 900 °C and 2.0 GPa: constraints on the trace element chemistry of mantle and deep crustal fluids, Geochim. Cosmochim. Acta 59 (1995) 3331–3350.
[58] T. Kogiso, Y. Tatsumi, S. Nakano, Trace element transport during dehydration processes in the subducted oceanic crust: 1. Experiments and implications for the origin of ocean island basalts, Earth Planet. Sci. Lett. 148 (1997) 193–205.
[59] H. Becker, K.P. Jochum, R.W. Carlson, Constraints from high-pressure veins in eclogites on the composition of hydrous fluids in subduction zones, Chem. Geol. 160 (1999) 291–308.
[60] H. Becker, K.P. Jochum, R.W. Carlson, Trace element fractionation during dehydration of eclogites from high-pressure terranes and the implications for element fluxes in subduction zones, Chem. Geol. 163 (2000) 65–99.
[61] T. Hammouda, High-pressure melting of carbonated eclogite and experimental constraints on carbon recycling and storage in the mantle, Earth Planet. Sci. Lett. 214 (2003) 357–368.
[62] R. Dasgupta, M.M. Hirschmann, A.C. Withers, Deep global cycling of carbon constrained by the solidus of anhydrous, carbonated eclogite under upper mantle conditions, Earth Planet. Sci. Lett. 227 (2004) 73–85.
[63] D.M. Kerrick, J.A.D. Connolly, Metamorphic devolatilization of subducted oceanic metabasalts: implications for seismicity, arc magmatism and volatile recycling, Earth Planet. Sci. Lett. 189 (2001) 19–29.
[64] O. Rouxel (pers. comm.).
[65] S.-S. Sun, W.F. McDonough, Chemical and isotopic systematics of oceanic basalts: implications for mantle composition and process, in: A.D. Saunders, M.J. Norry (Eds.), Magmatism in Ocean Basins, Spec. Publ.-Geol. Soc., vol. 42, pp. 313–345.
[66] D.A. Gust, R.J. Arculus, A.B. Kersting, Aspects of magma sources and processes in the Honshu Arc, Can. Mineral. 35 (1997) 347–365.
[67] T. Plank, Constraints from Thorium/Lanthanum on sediment recycling at subduction zones and the evolution of the continents, J. Petrol. (2005), doi:10.1093/petrology/egi005.